Direct Generation of Narrow-band Hyperentangled Photons

Tian-Ming Zhao,[*] Yong Sup Ihn, and Yoon-Ho Kim[†]

Department of Physics, Pohang University of Science and Technology (POSTECH), Pohang 37673, Korea

In quantum communication and photonic quantum information processing, the requirement of quantum repeaters and quantum memory often imposes a strict bandwidth prerequisite for the entangled photons. At the same time, there is ever more increasing demand for entangling more degrees of freedom, i.e., hyperentanglement, for a photon pair. In this Letter, we report the direct generation of narrow-band orbital angular momentum (OAM) and polarization hyperentangled photons from cold atoms. The narrow-band photon pair is naturally entangled in polarization and OAM, in addition to time-frequency, degrees of freedom due to spin and orbital angular momentum conservation conditions in the spontaneous four-wave mixing process in a cold atom ensemble. The narrow-band hyperentangled photon pair source reported here is expected to play important roles in quantum memory-based long-distance quantum communication.

An entangled photon source is one of the essential resources for quantum communication and photonic quantum computing. The two-photon state based on spontaneous parametric down-conversion (SPDC) in a second-order nonlinear crystal has been the workhorse in the photonic quantum information community for decades, providing useful bipartite entanglement in polarization [1,2], path [3–5], energy-time [6,7], position-momentum [8], orbital angular momentum (OAM) [9,10], as well as multipartite entanglement [11,12] and hyperentanglement [13,14]. The SPDC photons however have the spectral bandwidth on the order of several THz, making them incompatible with quantum memory and quantum repeaters based on atoms [15–18]. While optical cavities can be used to reduce the bandwidth of the SPDC photons, they introduce significant restrictions on the possibility of utilizing photons' external degrees of freedom (d.o.f.) [19–21].

An entangled photon source based on spontaneous four-wave mixing (SFWM) in an atomic medium is thus an ideal choice for a photon source compatible with atomic quantum memory [22,23]. The SFWM photon pair is naturally energy-time entangled [24,25] and can be made to exhibit polarization entanglement [26] and Einstein-Podolsky-Rosen position-momentum entanglement [27]. Demonstration of hyperentanglement, entanglement in multiple d.o.f. of a photon pair, is particularly of importance for cold-atom based narrow-band SFWM photons due to significantly lower photon flux than that of SPDC and, recently, hyperentanglement in polarization and time-energy d.o.f. from cold atoms has been demonstrated [26]. OAM states that can be defined in high-dimensional Hilbert space have been widely studied over the past years [28–32]. A variety of pioneering works in the OAM state in the atomic system have been reported recently, including

photon-generation and quantum memory [33–38]. Especially, polarization and OAM hyperentangled state was firstly generated from cold atoms, which relied on external interferometers, introducing undesired instability and complexity issues [39].

In this Letter, we report demonstration of, to the best of our knowledge, the first direct generation of narrow-band OAM-polarization hyperentanglement for a cold-atom based SFWM photon pair. The narrow-band photon pair is naturally entangled in polarization and OAM, in addition to time-frequency, d.o.f. due to spin and orbital angular momentum conservation conditions in the spontaneous four-wave mixing process in a cold atom ensemble. Our scheme does not involve any external interferometers and, therefore, the scheme is naturally stable. Also, owing to simplicity of the setup, the scheme offers higher-efficiency generation of OAM-polarization hyperentanglement. The narrow-band hyperentangled photon pair source reported here is expected to play an important role in quantum memory–based long-distance quantum communication.

We first describe the experimental setup for direct generation of narrow-band OAM-polarization hyperentangled photon pairs from SFWM in cold atoms. The experimental setup is illustrated in Fig. 1. The ^{87}Rb atoms are laser cooled and trapped in a magneto-optical trap (MOT) with an optical depth of $\sim$10 and the atoms are initially prepared in the state $|1\rangle$ [40]. The initial preparation process for the cold atom cloud takes 9 ms. For the next 1 ms, the MOT is turned off, releasing the cold atom cloud, and the counterpropagating pump and coupling laser beams are applied, causing Stokes and anti-Stokes photon pair generation via the spontaneous four-wave mixing process [22]. The pump beam is red detuned from the transition $|1\rangle \rightarrow |4\rangle$ by $\Delta = 60$ MHz with the power of 60 μW and the $1/e^2$ beam diameter of 1.8 mm.
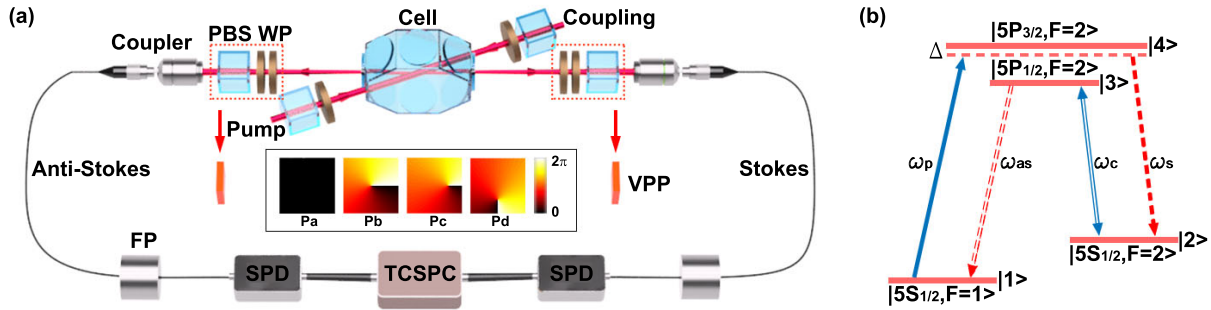
FIG. 1. System schematics. (a) Experimental setup for creation and detection of the hyperentangled state. WP is the wave plate, PBS is the polarization beam splitter, VPP is the vortex phase plate, FP is the Fabry-Perot cavity, SPD is the single-photon detector, and TCSPC is the time-correlated single-photon counting module. Coupler is the combination of objective lens and single mode fiber. In the inset, we show the phase pattern of the VPPs. Pa, Pb, Pc, and Pd are in sequence used to measure $|G\rangle$, $|R\rangle$, $1/\sqrt{2}(|G\rangle + |R\rangle)$ and $1/\sqrt{2}(|G\rangle - i|R\rangle)$ modes, see text for details. (b) The energy level diagram for SFWM.

The coupling beam is on resonance with the transition $|2\rangle \to |3\rangle$ with the power of 10 mW and the diameter of 1.8 mm. The polarization of the coupling and pump lasers are σ^+ and σ^-, respectively. Due to phase matching, counterpropagating Stokes and anti-Stokes photon pairs are generated between the transitions $|4\rangle \to |2\rangle$ and $|3\rangle \to |1\rangle$, respectively.

The Stokes and anti-Stokes photon pair is collected, at an angle of 3° relative to the pump and coupling beam directions, by using single mode optical fibers to spatially filter them from the strong pump and coupling laser beams. The bandwidth of the two-photons is 14.6(7) MHz. To further reduce noise photons from scattered pump or coupling lasers, a couple of temperature-controlled Fabry-Perot etalons with a bandwidth of 215 MHz are used as frequency filters. The transmittance of each etalon is 90%. The two-photon count rate is 42(6)/s. Note that the biphoton modes are focused in the middle of the Rb cell with the $1/e^2$ diameter of 250 μm.

One of the key advantages of our scheme is that the photon pair from SFWM is naturally hyperentangled in polarization and OAM d.o.f., in addition to time-energy entanglement. The polarization-OAM hyper-entanglement has been achieved by the judicious choice of polarization and OAM configurations of the pump and coupling beams. Generally speaking, only the total angular momentum is conserved during the SFWM process. However, spin angular momentum (SAM) and OAM can be separately conserved when a light beam propagates in a vacuum or a homogeneous and isotropic medium in the paraxial approximation [41,42]. Independent conservation of SAM and OAM states for the SFWM process in a cold atom ensemble without tightly focused beams allows us to achieve direct generation of narrow polarization-OAM hyper-entangled photons. Note that time-energy entanglement is also present in SFWM photon pairs, and it has been studied elsewhere [24,25].

Let us first discuss the mechanism for polarization entanglement of the SFWM photon pair in our case as

the scheme differs significantly from those of prior works reported in Ref. [26,39,43]. To date, polarization entanglement of the SFWM photon pair has been mainly achieved by the following two methods: (i) by using two separate SFWM pathways in a Mach-Zehnder interferometer [39,43] and (ii) by relying on the right-angle geometry for pump and coupling lasers and SFWM photons [26]. There are some obvious disadvantages with these schemes. For the first scheme [39,43], interferometric stability is required for generating polarization entanglement and long-term stability of a large Mach-Zehnder interferometer involving a cold atom medium is not trivial. For the latter [26], to achieve the right-angle geometry, large pump detuning and pump power is required. Our scheme makes use of SAM conversation to directly generate polarization entangled photon pairs from cold atoms [44].

After the cold atom ensemble is trapped in a MOT, we turn off the magnetic field and compensate for the stray magnetic fields so that the atoms are prepared in the ground state without Zeeman splitting. For SFWM photon pair generation, the weak pump laser and strong coupling laser beams are applied in the counterpropagating geometry to the cold atom ensemble, see Fig. 1(a). Since SFWM is a parametric process, after a transition cycle, the atoms come back to the initial states. Although the Zeeman sublevels are degenerate, the transitions between different Zeeman sublevels may generate photons with different polarization states. Table I describes all possible polarization combinations for the SFWM process involving the degenerate Zeeman sublevels. Note that, for a specific pump and coupling polarization combination, there exist two conjugate polarization pathways for the Stokes and anti-Stokes photons. If such a set of conjugate polarization pathways become indistinguishable, the two photons become polarization entangled.

Figure 2 shows the energy level diagrams and transition pathways for the SFWM processes that may result in direct generation of polarization entangled photon pairs. The transition pathways for σ^- polarized Stokes and σ^+

TABLE I. Polarization combinations for the involved photons. The second and third rows are for coupling with σ^+ and pump with σ^-. The fifth and sixth rows are for coupling with σ^- and pump with σ^+. For each combination, there exist two conjugate polarization pathways for the Stokes and anti-Stokes photons.

Coupling	Pump	Stokes	Anti-Stokes
σ^+	σ^+	σ^+	σ^+
σ^+	σ^-	σ^+	σ^-
σ^+	σ^-	σ^-	σ^+
σ^-	σ^-	σ^-	σ^-
σ^-	σ^+	σ^+	σ^-
σ^-	σ^+	σ^-	σ^+

polarized anti-Stokes photons are shown in Fig. 2(a). The transition pathways for σ^+ polarized Stokes and σ^- polarized anti-Stokes photons are shown in Fig. 2(b). The case in Fig. 2 contains exactly two biphoton amplitudes and therefore is our choice for directly generating polarization entangled photon pairs. As the Zeeman sublevels are degenerate, the two biphoton polarization amplitudes in Fig. 2 are degenerate, leading to the polarization entangled state,

$$|\psi\rangle_{\mathrm{SAM}} = \frac{1}{\sqrt{1+\gamma_1^2}}(|\sigma_s^+\sigma_{as}^-\rangle + \gamma_1|\sigma_s^-\sigma_{as}^+\rangle), \qquad (1)$$

where γ_1 represents the relative amplitude between $|\sigma_s^+\sigma_{as}^-\rangle$ and $|\sigma_s^-\sigma_{as}^+\rangle$ modes. The subscripts s and as refer to the Stokes and the anti-Stokes photons, respectively.

While it is convenient to describe polarization states in the atomic reference frame when atom-photon interaction is involved, for the propagating photons, it is more convenient to express the polarization states in the detector's reference frame. Considering the fact that Stokes and anti-Stokes photons are propagating in the opposite directions, the state in Eq. (1) should be rewritten in the detector's reference frame as,
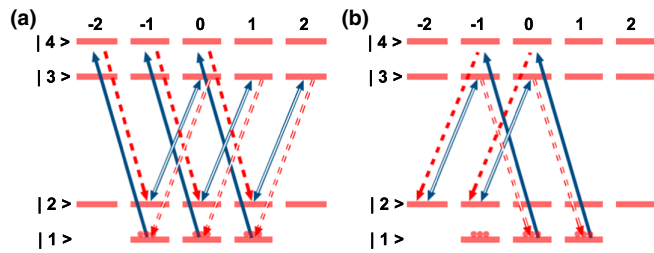

FIG. 2. Energy level diagrams and transition paths at different polarization configurations in SFWM when coupling and pump beam are with the polarization σ^+ and σ^-, respectively. (a) For σ^- polarized Stokes and σ^+ polarized anti-Stokes photons. (b) For σ^+ polarized Stokes and σ^- polarized anti-Stokes photons. Solid, double solid, dashed, and double dashed lines are transitions for the pump, coupling, Stokes photon, and anti-Stokes photons, respectively.

$$|\psi\rangle'_{\mathrm{SAM}} = \frac{1}{\sqrt{1+\gamma_1^2}}(|\sigma_s^+\sigma_{as}^+\rangle + \gamma_1|\sigma_s^-\sigma_{as}^-\rangle). \qquad (2)$$

Let us now discuss the entanglement in the OAM d.o.f. of the SFWM photons. Within the paraxial approximation, the spatial modes of the light beams carrying OAM are usually described by the Laguerre-Gaussian (LG_{pl}) function, where p and l represent the radial and azimuthal numbers, respectively. Due to OAM conservation, high dimensional bipartite entanglement is possible. When the coupling and pump beams are both carrying zero OAM, the OAM state of Stokes and anti-Stokes photons is entangled as

$$|\psi\rangle = C \sum_{m=-\infty}^{\infty} \alpha_m|m_s\rangle|-m_{as}\rangle, \qquad (3)$$

where C is the normalization coefficient and α_m is the relative amplitude of the state with OAM of $m\hbar$ [35,36]. As in Refs. [35,36], for simplicity, we focus on modes with $m = 0$ and 1. Hereafter, we describe states with OAM of 0, $\hbar$, and $-\hbar$ as $|G\rangle$, $|R\rangle$ and $|L\rangle$, respectively. Thus the expected entangled state can be written as

$$|\psi\rangle_{\mathrm{OAM}} = \frac{1}{\sqrt{1+\gamma_2^2}}(|G_sG_{as}\rangle + \gamma_2|R_sL_{as}\rangle), \qquad (4)$$

where γ_2 represents the relative amplitude. Again, we re-express the equation in terms of the detector's reference frame and considering the fact that Stokes and anti-Stokes photons are counterpropagating, Eq. (4) is rewritten as,

$$|\psi\rangle'_{\mathrm{OAM}} = \frac{1}{\sqrt{1+\gamma_2^2}}(|G_sG_{as}\rangle + \gamma_2|R_sR_{as}\rangle). \qquad (5)$$

The narrow-band SFWM biphoton state is therefore polarization-OAM hyperentangled, in addition to energy-time, and can be written as

$$|\psi\rangle = C(|\sigma_s^+\sigma_{as}^+\rangle + \gamma_1|\sigma_s^-\sigma_{as}^-\rangle) \otimes (|G_sG_{as}\rangle + \gamma_2|R_sR_{as}\rangle) \qquad (6)$$

where C is the normalization coefficient.

In order to confirm the hyperentanglement nature of the quantum state, we perform quantum state tomography for the polarization state as well as OAM states of the photons. First, for the polarization d.o.f., we apply the standard quantum state tomography technique using combinations of WPs and PBS in front of the coupling optics in the paths of Stokes and the anti-Stokes photons, see Fig. 1(a). The measurement bases are chosen as $|H\rangle$, $|V\rangle$, $|+\rangle = 1/\sqrt{2}(|H\rangle + |V\rangle)$ and $|\sigma^+\rangle = 1/\sqrt{2}(|H\rangle - i|V\rangle)$, where $|H\rangle$ and $|V\rangle$ represent the horizontal and vertical polarization, respectively. Note also that, in experiment, γ_1 in Eq. (2) is related to parameters of the MOT, alignment of all
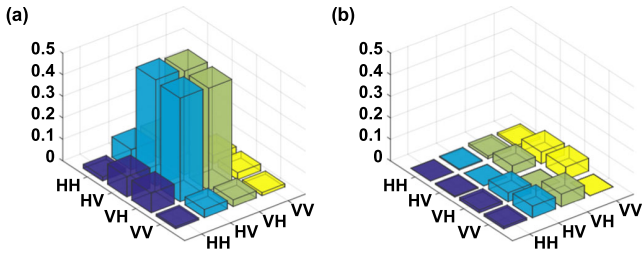
FIG. 3. Reconstructed two-photon polarization state ρ_1. The real and imaginary parts are shown in (a) and (b), respectively.

the beams and hyperfine dipole matrix elements [44–46]. The joint count rates are then used to reconstruct the density matrix ρ_1 by using the maximum likelihood method. The reconstructed polarization density matrix ρ_1 shown in Fig. 3. The density matrix ρ_1 exhibits purity $(\mathrm{Tr}[\rho^2])$ of 0.988(3) and tangle (Concurrence^2) of 0.952(5), confirming polarization entanglement of the photon pair. The experimentally obtained value of γ_1, from the density matrix, is $-0.692(5)$. The fidelity of ρ_1 to the maximally entanglement state $(|\sigma^+\sigma^+\rangle - |\sigma^-\sigma^-\rangle)/\sqrt{2}$ is 0.982(1).

To perform quantum state tomography for the OAM d.o.f., WPs and PBS used for the polarization measurement are now replaced with VPPs (vortex phase plate, VPP-1b, RPC Photonics Corp.). As we are analyzing for a two-dimensional state for each photon, the four projection measurement bases are defined as $|G\rangle$, $|R\rangle$, $1/\sqrt{2}(|G\rangle + |R\rangle)$, and $1/\sqrt{2}(|G\rangle - i|R\rangle)$. The phase patterns of the VPPs for four bases are illustrated in the inset of Fig. 1(a). The choice of measurement basis is implemented by translation or rotation of the VPPs [47,48]. To measure the Gauss mode $|G\rangle$, we use Pa which is a border area of the VPP containing no phase pattern. To measure the $|R\rangle$ mode, we use the Pb phase pattern of the VPP: the photon is injected through the center of the Pb phase pattern and then collected at a single-mode fiber. To perform the projection on the superposition basis $1/\sqrt{2}(|G\rangle + |R\rangle)$, the Pc phase pattern having an off-axis dislocation is used. Finally, projection measurement on the superposition basis $1/\sqrt{2}(|G\rangle - i|R\rangle)$ is made possible by Pd, having an off-axis dislocation that is rotated by 90° with respect to Pc.

The two-photon OAM density matrix ρ_2, reconstructed from the 16 coincidence measurements and the maximum

likelihood method, is shown in Fig. 4. From the density matrix, we obtain the purity and tangle of 0.969(4) and 0.922(8), respectively, and this confirms that the biphoton states exhibit two-dimensional OAM entanglement. The relative amplitude γ_2 is affected by different generation efficiencies between the LG_{00} and LG_{01} modes and by different transmissions of the VPPs during the projection measurement. The experimentally obtained value of γ_2 from the density matrix ρ_2 is 0.879(8). The fidelity of ρ_2 to the maximally entanglement state $(|GG\rangle + |RR\rangle)/\sqrt{2}$ is 0.985(1).

In summary, we report, to the best of our knowledge, the first direct generation of narrow-band orbital angular momentum (OAM)-polarization, in addition to energy-time entanglement, hyperentangled photons from cold atoms. Previous demonstrations of polarization entangled photons from cold atoms required an actively-phase locked Mach-Zehnder interferometer [39,43] or huge pump detuning and pump power for the right-angle geometry [26]. The novel scheme demonstrated here makes use of spin angular momentum and orbital angular momentum conservation during the SFWM process in cold atoms, resulting in a simplified experimental setup with low pump power requirement. The polarization-OAM hyperentanglement is confirmed with quantum state tomography, exhibiting a high degree of purity and entanglement of the photons. Although energy-time entanglement has not been tested in this Letter independently, based on prior work on the energy-time entangled nature of the SFWM photons from cold atoms [24,25,48], the scheme demonstrated in this Letter produces a narrow-band photon pair hyperentangled in polarization, OAM, and energy-time d.o.f. Considering the bandwidth requirement for efficient atom-photon interaction, which is at the heart of quantum repeaters and quantum memory, hyperentanglement of multiple d.o.f. for a narrow-band photon pair is of significant importance in photonic quantum information. The narrow-band hyperentangled photon pair source reported here is expected to play important roles in quantum memory–based long-distance quantum communication.
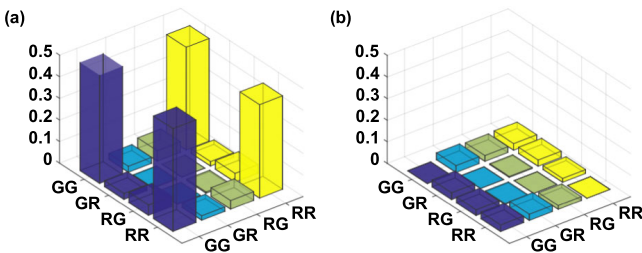
FIG. 4. Reconstructed two-photon OAM state ρ_2. The real and imaginary parts are shown in (a) and (b), respectively.

[*] timmizhao@gmail.com
[†] yoonho72@gmail.com

[1] P. G. Kwiat, K. Mattle, H. Weinfurter, A. Zeilinger, A. V. Sergienko, and Y. Shih, Phys. Rev. Lett. **75**, 4337 (1995).
[2] Y.-H. Kim, S. P. Kulik, M. V. Chekhova, W. P. Grice, and Y. Shih, Phys. Rev. A **67**, 010301(R) (2003).
[3] K. Edamatsu, R. Shimizu, and T. Itoh, Phys. Rev. Lett. **89**, 213601 (2002).
[4] M. W. Mitchell, J. S. Lundeen, and A. M. Steinberg, Nature (London) **429**, 161 (2004).

[5] Y.-S. Kim, O. Kwon, S. M. Lee, J.-C. Lee, H. Kim, S.-K. Choi, H. S. Park, and Y.-H. Kim, Opt. Express **19**, 24957 (2011).

[6] J. Brendel, N. Gisin, W. Tittel, and H. Zbinden, Phys. Rev. Lett. **82**, 2594 (1999).

[7] L. K. Shalm, D. R. Hamel, Z. Yan, C. Simon, K. J. Resch, and T. Jennewein, Nat. Phys. **9**, 19 (2013).

[8] M. D'Angelo, Y.-H. Kim, S. P. Kulik, and Y. Shih, Phys. Rev. Lett. **92**, 233601 (2004).

[9] A. Mair, A. Vaziri, G. Weihs, and A. Zeilinger, Nature (London) **412**, 313 (2001).

[10] Z.-Y. Zhou, S.-L. Liu, Y. Li, D.-S. Ding, W. Zhang, S. Shi, M.-X. Dong, B.-S. Shi, and G.-C. Guo, Phys. Rev. Lett. **117**, 103601 (2016).

[11] X.-C. Yao, T.-X. Wang, P. Xu, H. Lu, G.-S. Pan, X.-H. Bao, C.-Z. Peng, C.-Y. Lu, Y.-A. Chen, and J.-W. Pan, Nat. Photonics **6**, 225 (2012).

[12] X.-L. Wang, L.-K. Chen, W. Li, H.-L. Huang, C. Liu, C. Chen, Y.-H. Luo, Z.-E. Su, D. Wu, Z.-D. Li, H. Lu, Y. Hu, X. Jiang, C.-Z. Peng, L. Li, N.-L. Liu, Y.-A. Chen, C.-Y. Lu, and J.-W. Pan, Phys. Rev. Lett. **117**, 210502 (2016).

[13] J. T. Barreiro, T.-C. Wei, and P. G. Kwiat, Nat. Phys. **4**, 282 (2008).

[14] X.-L. Wang, Y.-H. Luo, H.-L. Huang, M.-C. Chen, Z.-E. Su, C. Liu, C. Chen, W. Li, Y.-Q. Fang, X. Jiang, J. Zhang, L. Li, N.-L. Liu, C.-Y. Lu, and J.-W. Pan, Phys. Rev. Lett. **120**, 260502 (2018).

[15] L.-M. Duan, M. D. Lukin, J. I. Cirac, and P. Zoller, Nature (London) **414**, 413 (2001).

[16] K. S. Choi, H. Deng, J. Laurat, and H. J. Kimble, Nature (London) **452**, 67 (2008).

[17] X.-H. Bao, A. Reingruber, P. Dietrich, J. Rui, A. Dück, T. Strassel, L. Li, N.-L. Liu, B. Zhao, and J.-W. Pan, Nat. Phys. **8**, 517 (2012).

[18] K.-K. Park, Y.-W. Cho, Y.-T. Chough, and Y.-H. Kim, Phys. Rev. X **8**, 021016 (2018).

[19] Z. Y. Ou and Y. J. Lu, Phys. Rev. Lett. **83**, 2556 (1999).

[20] X.-H. Bao, Y. Qian, J. Yang, H. Zhang, Z.-B. Chen, T. Yang, and J.-W. Pan, Phys. Rev. Lett. **101**, 190501 (2008).

[21] T.-M. Zhao, H. Zhang, J. Yang, Z.-R. Sang, X. Jiang, X.-H. Bao, and J.-W. Pan, Phys. Rev. Lett. **112**, 103602 (2014).

[22] V. Balić, D. A. Braje, P. Kolchin, G. Y. Yin, and S. E. Harris, Phys. Rev. Lett. **94**, 183601 (2005).

[23] C. Shu, P. Chen, T. K. A. Chow, L. Zhu, Y. Xiao, M. M. T. Loy, and S. Du, Nat. Commun. **7**, 12783 (2016).

[24] Y.-W. Cho, K.-K. Park, J.-C. Lee, and Y.-H. Kim, Phys. Rev. Lett. **113**, 063602 (2014).

[25] K.-K. Park, J.-H. Kim, T.-M. Zhao, Y.-W. Cho, and Y.-H. Kim, Optica **4**, 1293 (2017).

[26] H. Yan, S. Zhang, J. F. Chen, M. M. T. Loy, G. K. L. Wong, and S. Du, Phys. Rev. Lett. **106**, 033601 (2011).

[27] J.-C. Lee, K.-K. Park, T.-M. Zhao, and Y.-H. Kim, Phys. Rev. Lett. **117**, 250501 (2016).

[28] M. Erhard, R. Fickler, M. Krenn, and A. Zeilinger, Light: Sci. Amp. Appl. **7**, 17146 (2018), review Article.

[29] A. Babazadeh, M. Erhard, F. Wang, M. Malik, R. Nouroozi, M. Krenn, and A. Zeilinger, Phys. Rev. Lett. **119**, 180510 (2017).

[30] M. Mafu, A. Dudley, S. Goyal, D. Giovannini, M. McLaren, M. J. Padgett, T. Konrad, F. Petruccione, N. Lütkenhaus, and A. Forbes, Phys. Rev. A **88**, 032305 (2013).

[31] V. Parigi, V. D'Ambrosio, C. Arnold, L. Marrucci, F. Sciarrino, and J. Laurat, Nat. Commun. **6**, 7706 (2015), article.

[32] M. Prilmüller, T. Huber, M. Müller, P. Michler, G. Weihs, and A. Predojević, Phys. Rev. Lett. **121**, 110503 (2018).

[33] R. F. Offer, D. Stulga, E. Riis, S. Franke-Arnold, and A. S. Arnold, Commun. Phys. **1**, 84 (2018).

[34] D.-S. Ding, M.-X. Dong, W. Zhang, S. Shi, Y.-C. Yu, Y.-H. Ye, G.-C. Guo, and B.-S. Shi, arXiv:1806.10407.

[35] Q.-F. Chen, B.-S. Shi, Y.-S. Zhang, and G.-C. Guo, Phys. Rev. A **78**, 053810 (2008).

[36] R. Inoue, N. Kanai, T. Yonehara, Y. Miyamoto, M. Koashi, and M. Kozuma, Phys. Rev. A **74**, 053809 (2006).

[37] A. Nicolas, L. Veissier, L. Giner, E. Giacobino, D. Maxein, and J. Laurat, Nat. Photonics **8**, 234 (2014).

[38] G. Walker, A. S. Arnold, and S. Franke-Arnold, Phys. Rev. Lett. **108**, 243601 (2012).

[39] W. Zhang, D.-S. Ding, M.-X. Dong, S. Shi, K. Wang, S.-L. Liu, Y. Li, Z.-Y. Zhou, B.-S. Shi, and G.-C. Guo, Nat. Commun. **7**, 13514 (2016).

[40] K.-K. Park, Y.-T. Chough, and Y.-H. Kim, J. Korean Phys. Soc. **70**, 1007 (2017).

[41] L. Marrucci, C. Manzo, and D. Paparo, Phys. Rev. Lett. **96**, 163905 (2006).

[42] Y. Zhao, J. S. Edgar, G. D. M. Jeffries, D. McGloin, and D. T. Chiu, Phys. Rev. Lett. **99**, 073901 (2007).

[43] K. Liao, H. Yan, J. He, S. Du, Z.-M. Zhang, and S.-L. Zhu, Phys. Rev. Lett. **112**, 243602 (2014).

[44] G. K. Gulati, B. Srivathsan, B. Chng, A. Cerè, and C. Kurtsiefer, New J. Phys. **17**, 093034 (2015).

[45] S. Du, J. Wen, and M. H. Rubin, J. Opt. Soc. Am. B **25**, C98 (2008).

[46] Y.-W. Cho, K.-K. Park, J.-C. Lee, and Y.-H. Kim, J. Korean Phys. Soc. **63**, 943 (2013).

[47] Z.-Q. Zhou, Y.-L. Hua, X. Liu, G. Chen, J.-S. Xu, Y.-J. Han, C.-F. Li, and G.-C. Guo, Phys. Rev. Lett. **115**, 070502 (2015).

[48] See Supplemental Material at http://link.aps.org/supplemental/10.1103/PhysRevLett.122.123607 for the time-frequency entanglement and the adjustment of the VPPs.